Electronic Supplementary Information: Field-Dependent THz Transport Nonlinearities in Semiconductor Nano Structures

Quentin Wach,[a] Michael T. Quick,[a] Sabrine Ayari[b] and Alexander W. Achtstein[a,c*]

[a] *Institute of Optics and Atomic Physics, Technische Universität Berlin, 10623 Berlin, Germany*

[b] *Laboratoire de Physique de l'École normale supérieure, ENS, Université PSL, CNRS, Sorbonne Université, Université Paris-Diderot, Sorbonne Paris Cité, Paris, France*

[c] *Fakultät für Physik, Universität Bielefeld, Universitätsstr. 25, 33615 Bielefeld, Germany; E-mail: achtstein@physik.uni-bielefeld.de*

CONTENTS

S1. RELAXATION RATE COEFFICIENTS

The rates for electron or hole scattering by longitudinal acoustical LA Phonons from initial state $|\psi_\nu^i\rangle$ with energy E_ν^i to final states $|\psi_\nu^f\rangle$ with energy E_ν^f, are calculated in first-order perturbation theory using the Fermi golden rule as follows :

$$\Gamma_\nu^{i\to f} = \frac{2\pi}{\hbar}\sum_{\boldsymbol{q}} \left|\left\langle \Psi^i \left| \mathbb{H}_{\nu-ph}^{LA} \right| \Psi^f \right\rangle\right|^2 \delta\left(E_\nu^f - E_\nu^i \mp E_{LA}(q)\right) \tag{S1}$$

where $q = (q_x, q_y, q_z)$ is the phonon wave vector, $\nu = e, h$, for electron and hole, respectively. The upper (lower) signs in the δ function account for emission (absorption) of phonons by an electron in the initial quantum state i. The electron-phonon interaction Hamiltonian is given by :

$$H_{\nu-ph}^{LA} = V_{LA}(q) e^{\mp i\boldsymbol{q}\cdot\boldsymbol{r_\nu}} \hat{a}_{LA,\boldsymbol{q}}^{+} + c.c. \tag{S2}$$

Here, $\hat{a}_{LA,\boldsymbol{q}}^{+}$ ($\hat{a}_{LA,\boldsymbol{q}}$) are the phonon creation (annihilation) operators for mode LA with wave vector $\boldsymbol{q}$. The coupling of electrons/hole to longitudinal-acoustic (LA) phonons by means of a deformation potential D_ν is described by:

$$V_\nu^{LA}(q) = \frac{D_\nu}{\sqrt{2\rho_d c_s^2 V}}\sqrt{E_{LA}(q)}, \tag{S3}$$

where $E_{LA}(q) = \hbar\omega_q = \hbar c_s q$ is the LA phonon energy, $V = L_x L_y L_z$ is the quantization volume, ρ_d is the mass density, c_s is the longitudinal velocity of sound. The initial and final state is given by :

$$|\Psi^i\rangle = \left|\psi_\nu^i\right\rangle \otimes |N_{q,LA}\rangle_{\boldsymbol{q}}$$
$$|\Psi^f\rangle = \left|\psi_\nu^f\right\rangle \otimes |N_{q,LA} \pm 1\rangle_{\boldsymbol{q}}$$

where $|N_{q,LA}\rangle_{\boldsymbol{q}}$ is the number state of the phonon mode with wavevector $\boldsymbol{q}$.

The corresponding electronic part of the wavefunction is given by particle-in-a-box type states, i.e.

$$\begin{aligned}|\psi_\nu^{i(f)}\rangle = |\psi_\nu^{i(f)}(x,y,z)\rangle &= \sqrt{\frac{2}{L_x}}\sin\left(\frac{n_x^{i(f)}\pi x}{L_x}\right) \times \sqrt{\frac{2}{L_y}}\sin\left(\frac{n_y^{i(f)}\pi y}{L_y}\right) \times \sqrt{\frac{2}{L_z}}\sin\left(\frac{n_z^{i(f)}\pi z}{L_z}\right) \\ &= \sqrt{\frac{8}{V}}\sin\left(\frac{n_x^{i(f)}\pi x}{L_x}\right)\sin\left(\frac{n_y^{i(f)}\pi y}{L_y}\right)\sin\left(\frac{n_z^{i(f)}\pi z}{L_z}\right).\end{aligned} \tag{S4}$$

Due to the rather low charge carrier masses compared to the lateral extensions of the nanostructures, the quantized wavefunctions apply in every case - even the longest nanorod of 40 nm length.

The occupation number is given by the Bose distribution $N_{LA}(q,T) = \left[\exp\left(\frac{E_{LA}(q)}{K_B T}\right) - 1\right]^{-1}$. The delta functions $\delta\left(E_\nu^f - E_\nu^i \pm E_{LA}(q)\right)$ ensure the energy conservation for inelastic scattering processes by the absorption or emission of phonons of energy $E_{LA}(q)$.

$$\langle\Psi^i|H_{\nu,ph}^{LA}|\Psi^f\rangle = \sqrt{\left(N_{LA}(q,T) + \frac{1}{2} \pm \frac{1}{2}\right)} V_\nu^{LA}(\boldsymbol{q}) \langle\psi_\nu^i| e^{\mp i\boldsymbol{q}\cdot\boldsymbol{r_\nu}} |\psi_\nu^f\rangle \tag{S5}$$

The sum over all the $\boldsymbol{q}$ vectors in Eq S1 can be expressed as an integral over $\boldsymbol{q}$, replacing Eq.S2, (S3) and (S5) in Eq(S1) we find:

$$\Gamma_{\nu}^{i\to f} = \frac{D_{\nu}^{2}}{2(2\pi)^{2}\rho_{d}\hbar c_{s}^{2}} \iiint \mathrm{d}q_{x}\mathrm{d}q_{y}\mathrm{d}q_{z} \left(N_{LA}(q,T) + \frac{1}{2} \pm \frac{1}{2}\right) E_{LA}(q_{x},q_{y},q_{z}) \left|\langle\psi_{\nu}^{i}|e^{-i\boldsymbol{q}\cdot\boldsymbol{r_{\nu}}}|\psi_{\nu}^{f}\rangle\right|^{2} \delta\left(E_{\nu}^{f} - E_{\nu}^{i} \mp E_{LA}(q)\right) \quad \text{(S6)}$$

In our work, we treat the structures as cuboids in the strong confinement regime. The confinement is modeled by potential barriers of infinite height outside the particle region. This particular choice of the confinement potential results in a complete separation of the carrier motion in the three spatial directions.

The matrix element is given by:

$$\begin{aligned}\langle\psi_{\nu}^{i}|e^{-i\boldsymbol{q}\cdot\boldsymbol{r_{\nu}}}|\psi_{\nu}^{f}\rangle &= \langle\phi_{z_{\nu}}^{i}|e^{-iq_{z}\cdot z_{\nu}}|\phi_{z_{\nu}}^{f}\rangle \times \langle\phi_{x_{\nu}}^{i}|e^{-iq_{x}\cdot x_{\nu}}|\phi_{x_{\nu}}^{f}\rangle \times \langle\phi_{y_{\nu}}^{i}|e^{-iq_{y}\cdot y_{e}}|\phi_{y_{\nu}}^{f}\rangle \\ &= \mathbb{F}^{\nu}_{n_{x}^{i},n_{x}^{f}}(q_{x}) \times \mathbb{F}^{\nu}_{n_{y}^{i},n_{y}^{f}}(q_{y}) \times \mathbb{F}^{\nu}_{n_{z}^{i},n_{z}^{f}}(q_{z}) \end{aligned} \quad \text{(S7)}$$

$$\mathbb{F}^{\nu}_{n_{\eta}^{i},n_{\eta}^{f}}(q_{\eta}) = \frac{sin\left(\frac{n_{\eta}^{i}\pi + n_{\eta}^{f}\pi + q_{\eta}L_{\eta}}{2}\right)}{n_{\eta}^{i}\pi + n_{\eta}^{f}\pi + q_{\eta}L_{\eta}} + \frac{sin\left(\frac{n_{\eta}^{f}\pi + q_{\eta}L_{\eta} - n_{\eta}^{i}\pi}{2}\right)}{n_{\eta}^{f}\pi + q_{\eta}L_{\eta} - n_{\eta}^{i}\pi} + \frac{sin\left(\frac{n_{\eta}^{i}\pi - n_{\eta}^{f}\pi + q_{\eta}L_{\eta}}{2}\right)}{n_{\eta}^{i}\pi - n_{\eta}^{f}\pi + q_{x(y)}L_{x(y)}} + \frac{sin\left(\frac{n_{\eta}^{i}\pi + n_{\eta}^{f}\pi - q_{\eta}L_{\eta}}{2}\right)}{n_{\eta}^{i}\pi + n_{\eta}^{f}\pi - q_{\eta}L_{\eta}} \quad \text{(S8)}$$

As seen from Eq.S8, $\mathbb{F}^{\nu}_{n_{\eta}^{i},n_{\eta}^{f}}(q_{\eta})$ decreases rapidly with increasing $q_{\eta}L_{\eta} \gg 1$. For small, q_{η}, it approaches zero and unity for interband $\left(n_{\eta}^{i} \neq n_{\eta}^{f}\right)$ and intraband $\left(n_{\eta}^{i} = n_{\eta}^{f}\right)$ transitions, respectively. The matrix element reduces to the conservation of the crystal momentum $\left[\delta\left(k_{i}^{\nu} - k_{f}^{\nu} + q\right)\right]$ for the case of an unconfined direction (for example laterally infinite TMDCs), where $k_{i(f)}^{\nu}$ is the initial (final) electron/hole wave vector. For $n_{\alpha}^{i} = n_{\alpha}^{f} = 1$, the matrix element $\mathbb{F}^{\nu}_{n_{\eta}^{i},n_{\eta}^{f}}(q_{\eta})$ can be written as :

$$\mathbb{F}_{11}^{\nu}(q_{\eta}) = \frac{\pi^{2}\sin(\frac{q_{\eta}L_{\eta}}{2})}{\frac{q_{\eta}L_{\eta}}{2}\left[\pi^{2} - (\frac{q_{\eta}L_{\eta}}{2})^{2}\right]}, \quad \text{(S9)}$$

The scattering rate is rewritten :

$$\Gamma_{\nu}^{i\to f} = \frac{D_{\nu}^{2}}{2(2\pi)^{2}\rho_{d}\hbar c_{s}^{2}} \iiint \left|\mathbb{F}_{LA}^{\nu}(q_{x},q_{y},q_{z})\right|^{2} E_{LA}(q_{x},q_{y},q_{z})\delta\left(E_{\nu}^{f} - E_{\nu}^{i} \mp E_{LA}(q)\right)\mathrm{d}q_{x}\mathrm{d}q_{y}\mathrm{d}q_{z} \quad \text{(S10)}$$

After taking advantage of the δ functions, which stands for the conservation of the total energy, we have evaluated Eq. S10 numerically for LA phonon scattering. In table S1-S6, we calculate the electron or hole-Phonon scattering rate of three different sizes of CdSe nanoparticles ($6 \times 6 \times 6\,\mathrm{nm}^3$, $20 \times 6 \times 6\,\mathrm{nm}^3$ and $40 \times 6 \times 6\,\mathrm{nm}^3$) for several transitions and for three different temperatures $T = 10\,\mathrm{K}, 70\,\mathrm{K}, 300\,\mathrm{K}$.

TABLE S1. The energy difference, the absorption (up) and emission (down)-scattering rates for electron-longitudinal acoustic phonon (LA) interaction for $6 \times 6 \times 6\,\mathrm{nm}^3$ size.

$\|i\rangle \leftrightarrow \|f\rangle$	ΔE (eV)	Γ_e^{UC} (ps^{-1})			Γ_e^{DC} (ps^{-1})		
		300 K	70 K	10 K	300 K	70 K	10K
$\|1\rangle \leftrightarrow \|2\rangle$	0.18	0.33	$6.1 \cdot 10^{-2}$	$1.4 \cdot 10^{-3}$	0.375	0.1076	$4.8 \cdot 10^{-2}$
$\|1\rangle \leftrightarrow \|3\rangle$	0.35	$5.7 \cdot 10^{-2}$	$1 \cdot 10^{-2}$	$1.4 \cdot 10^{-4}$	$6.7 \cdot 10^{-2}$	$2 \cdot 10^{-2}$	$1 \cdot 10^{-2}$
$\|1\rangle \leftrightarrow \|4\rangle$	0.464	$4.7 \cdot 10^{-2}$	$8.1 \cdot 10^{-3}$	$7.7 \cdot 10^{-5}$	$5.5 \cdot 10^{-2}$	$1.6 \cdot 10^{-2}$	$8.8 \cdot 10^{-3}$
$\|2\rangle \leftrightarrow \|3\rangle$	0.18	0.23	$4.2 \cdot 10^{-2}$	$9.8 \cdot 10^{-4}$	0.27	$7.8 \cdot 10^{-2}$	$3.7 \cdot 10^{-2}$
$\|2\rangle \leftrightarrow \|4\rangle$	0.29	0.11	$2.2 \cdot 10^{-2}$	$9.1 \cdot 10^{-4}$	0.123	$3.4 \cdot 0^{-2}$	$1.3 \cdot 10^{-2}$
$\|3\rangle \leftrightarrow \|4\rangle$	0.116	0.6	0.11	$2.65 \cdot 10^{-3}$	0.69	0.2	$9.35 \cdot 10^{-2}$

TABLE S2. The energy difference, the absorption (up) and emission (down)-scattering rates for electron-longitudinal acoustic phonon (LA) interaction for $20 \times 6 \times 6\,\mathrm{nm}^3$ size.

$\|i\rangle \leftrightarrow \|f\rangle$	ΔE (eV)	Γ_e^{UC} (ps^{-1})			Γ_e^{DC} (ps^{-1})		
		300 K	70 K	10 K	300 K	70 K	10K
$\|1\rangle \leftrightarrow \|2\rangle$	$1.56 \cdot 10^{-2}$	6.7	1.36	$6.2 \cdot 10^{-2}$	7.3	1.95	0.652
$\|1\rangle \leftrightarrow \|3\rangle$	$4.18 \cdot 10^{-2}$	2.325	0.465	$1.83 \cdot 10^{-2}$	2.55	0.69	0.20
$\|1\rangle \leftrightarrow \|4\rangle$	7.8310^{-2}	0.9	0.18	$6.48 \cdot 10^{-3}$	0.99	0.27	$9.01 \cdot 10^{-2}$
$\|2\rangle \leftrightarrow \|3\rangle$	2.610^{-2}	3.16	0.64	$3.2 \cdot 10^{-2}$	3.42	0.9	0.30
$\|2\rangle \leftrightarrow \|4\rangle$	$6.26 \cdot 10^{-2}$	0.94	0.19	$8.56 \cdot 10^{-3}$	1.02	0.27	$9.1 \cdot 10^{-2}$
$\|3\rangle \leftrightarrow \|4\rangle$	$3.65 \cdot 10^{-2}$	2.45	0.5	$2.5 \cdot 10^{-2}$	2.65	0.7	0.23

TABLE S3. The energy difference, the absorption (up) and emission (down)-scattering rates for electron-longitudinal acoustic phonon (LA) interaction for $40 \times 6 \times 6\,\mathrm{nm}^3$ size.

$\|i\rangle \leftrightarrow \|f\rangle$	ΔE (eV)	Γ_e^{UC} (ps^{-1})			Γ_e^{DC} (ps^{-1})		
		300 K	70 K	10 K	300 K	70 K	10K
$\|1\rangle \leftrightarrow \|2\rangle$	3.9210^{-3}	15.16	3.1	0.15	16.42	4.35	1.41
$\|1\rangle \leftrightarrow \|3\rangle$	1.0410^{-2}	4.04	0.82	$4.04 \cdot 10^{-2}$	4.38	1.16	0.378
$\|1\rangle \leftrightarrow \|4\rangle$	1.9510^{-2}	1.03	0.21	$9.59 \cdot 10^{-3}$	1.12	0.30	0.10
$\|2\rangle \leftrightarrow \|3\rangle$	$6.528 \cdot 10^{-3}$	8.05	1.63	7.8310^{-2}	8.76	2.33	0.78
$\|2\rangle \leftrightarrow \|4\rangle$	$1.56 \cdot 10^{-2}$	2.04	0.42	$2.1 \cdot 10^{-2}$	2.21	0.60	0.19
$\|3\rangle \leftrightarrow \|4\rangle$	$9.14 \cdot 10^{-3}$	4.32	0.88	$4.42 \cdot 10^{-2}$	4.68	1.24	0.41

TABLE S4. The energy difference, the absorption (up) and emission (down)-scattering rate for hole-longitudinal acoustic phonon (LA) interaction for $6 \times 6 \times 6\,\mathrm{nm}^3$ size.

$\|i\rangle \leftrightarrow \|f\rangle$	ΔE (eV)	Γ_h^{UC} (ps^{-1})			Γ_h^{DC} (ps^{-1})		
		300 K	70 K	10 K	300 K	70 K	10K
$\|1\rangle \leftrightarrow \|2\rangle$	4.01710^{-2}	2.23	0.413	$9.28 \cdot 10^{-3}$	2.55	0.73	0.32
$\|1\rangle \leftrightarrow \|3\rangle$	$8.03 \cdot 10^{-2}$	0.71	0.12	$1.74 \cdot 10^{-3}$	0.84	0.25	0.128
$\|1\rangle \leftrightarrow \|4\rangle$	0.107	0.36	$6.26 \cdot 10^{-2}$	$5.98 \cdot 10^{-4}$	0.43	0.13	$6.87 \cdot 10^{-2}$
$\|2\rangle \leftrightarrow \|3\rangle$	4.01710^{-2}	1.59	0.28	$6.41 \cdot 10^{-3}$	1.85	0.55	0.26
$\|2\rangle \leftrightarrow \|4\rangle$	$6.69 \cdot 10^{-2}$	0.81	0.15	$6.53 \cdot 10^{-3}$	0.89	0.24	$9.52 \cdot 10^{-2}$
$\|3\rangle \leftrightarrow \|4\rangle$	$2.67 \cdot 10^{-2}$	2.34	0.43	$9.96 \cdot 10^{-3}$	2.7	0.78	0.36

TABLE S5. The energy difference, the absorption (up) and emission (down)-scattering rate for hole-longitudinal acoustic phonon (LA) interaction for $20 \times 6 \times 6\,\mathrm{nm}^3$ size.

$\|i\rangle \leftrightarrow \|f\rangle$	ΔE (eV)	Γ_h^{UC} (ps^{-1})			Γ_h^{DC} (ps^{-1})		
		300 K	70 K	10 K	300 K	70 K	10K
$\|1\rangle \leftrightarrow \|2\rangle$	$3.615 \cdot 10^{-3}$	9.02	1.82	$8.11 \cdot 10^{-2}$	9.82	2.62	0.88
$\|1\rangle \leftrightarrow \|3\rangle$	$9.642 \cdot 10^{-3}$	2.32	0.46	$1.83 \cdot 10^{-2}$	2.54	0.68	0.23
$\|1\rangle \leftrightarrow \|4\rangle$	$1.81 \cdot 10^{-2}$	0.95	0.18	$6.58 \cdot 10^{-3}$	1.04	0.28	0.10
$\|2\rangle \leftrightarrow \|3\rangle$	6.02610^{-3}	4.4	0.88	$3.93 \cdot 10^{-2}$	4.82	1.29	0.44
$\|2\rangle \leftrightarrow \|4\rangle$	$1.44 \cdot 10^{-2}$	1.14	0.23	$1.02 \cdot 10^{-2}$	1.24	0.33	0.11
$\|3\rangle \leftrightarrow \|4\rangle$	$8.437 \cdot 10^{-3}$	2.63	0.53	$2.56 \cdot 10^{-2}$	2.86	0.76	0.25

TABLE S6. The energy difference and the absorption (up) and emission (down)-scattering rate for hole-longitudinal acoustic phonon (LA) interaction for $40 \times 6 \times 40\,\mathrm{nm}^3$ size.

$\|i\rangle \leftrightarrow \|f\rangle$	ΔE (eV)	Γ_h^{UC} (ps^{-1})			Γ_h^{DC} (ps^{-1})		
		300 K	70 K	10 K	300 K	70 K	10K
$\|1\rangle \leftrightarrow \|2\rangle$	9.0410^{-4}	12.15	2.55	0.15	16.4	4.19	1.12
$\|1\rangle \leftrightarrow \|3\rangle$	2.410^{-3}	4.72	0.97	$5.74 \cdot 10^{-2}$	5.11	1.35	0.44
$\|1\rangle \leftrightarrow \|4\rangle$	4.510^{-3}	2.83	0.57	$2.59 \cdot 10^{-2}$	3.09	0.82	0.27
$\|2\rangle \leftrightarrow \|3\rangle$	1.510^{-3}	6.58	1.36	$7.36 \cdot 10^{-2}$	7.07	1.85	0.56
$\|2\rangle \leftrightarrow \|4\rangle$	3.6210^{-3}	3.91	0.75	$2.02 \cdot 10^{-2}$	4.38	1.22	0.40
$\|3\rangle \leftrightarrow \|4\rangle$	$2.1 \cdot 10^{-3}$	4.7	0.96	$5.08 \cdot 10^{-2}$	5.072	1.33	0.42

TABLE S7. The material parameters used in the calculations: m_0 is the free electron mass.

$m_e =$ 0.18 m_0 [1]	$D_h =$ 0.76 eV [2, 3]
$m_h =$ 0.78 m_0 [4]	$c_s =$ 3860 m/s [5]
$D_e =$ -1.52 eV [2, 3]	$\rho_d =$ 5810 Kg/m^3 [6]

In the following section we discuss our scattering rate results with respect to literature. Our results on the phonon scattering rates are in-line with published experimental and theoretical findings, validating the accuracy of our approach. In reference Ref.[7] the authors have measured a scattering rate of 0.27 ps^{-1} at room temperature for the lowest state in a 6 nm CdSe nanoparticle. This is in good agreement with the obtained value of 0.33 ps^{-1} for the lowest $|1\rangle \rightarrow |2\rangle$ electron transition for 6 nm cuboids at room temperature in our study. Furthermore, Guyot-Sionnest et al., observed in ref. [8] a fast relaxation time of 0.16 ps^{-1} for 6 nm CdSe colloidal quantum dots using infrared pump-probe measurements, corroborating our results. Makkar et al. (Ref. [9]) reported for 12 nm dots at room temperature a cooling time of 650 fs, corresponding to rates of $\sim$1.5 ps^{-1}. We note the similar order of magnitude with respect to our scattering rates, with discrepancies potentially attributable to differences in nanocrystal size and shape, as the scattering rate e.g. strongly depends on nanocrystal size [10]. Our above presented calculation results are based on semi-analytical models for the phonon scattering the authors already introduced in Ref. [11], knowing that it gives appropriate results for CdSe based nano systems (as referring to phonon scattering rates and energies), in agreement with experimental measurements and published literature.

S2. MOBILITY PEAK MAXIMUM AND LINEWIDTH

Starting with Equation

$$\mu_{2LS} = -\mathbb{i}\frac{\omega}{\hbar q_e}(\rho_{11}^{eq} - \rho_{22}^{eq})|M_{21}|^2 \frac{(\omega - \omega_{21}) + \mathbb{i}\gamma_{21}}{(\omega - \omega_{21})^2 + \gamma_{21}^2 + 4\,G\,\Omega^2} \tag{S11}$$

from the main text, where again $G = \gamma_{21}/(\Gamma_{21} + \Gamma_{12})$ the ratio of dephasing and relaxation rate coefficients, we first extract its real part as focus of the discussion ahead

$$\mathrm{Re}\left\{\mu_{2LS}\right\} = -\mathbb{i}\frac{\omega}{\hbar q_e}(\rho_{11}^{eq} - \rho_{22}^{eq})|M_{21}|^2 \frac{(\omega - \omega_{21}) + \mathbb{i}\gamma_{21}}{(\omega - \omega_{21})^2 + \gamma_{21}^2 + 4\,G\,\Omega^2}. \tag{S12}$$

From here, in order to describe the position of the Lorentzian line maximum (the peak), we first form the derivative with respect to ω and set it zero

$$\frac{\mathrm{d}}{\mathrm{d}\omega}\mathrm{Re}\left\{\mu_{2LS}\right\} = \frac{\gamma_{21}}{\hbar q_e}(\rho_{11}^{eq} - \rho_{22}^{eq})|M_{21}|^2 \frac{\gamma_{21}^2 + 4\,G\,\Omega^2 - (\omega - \omega_{21})(\omega + \omega_{21})}{\left[(\omega - \omega_{21})^2 + \gamma_{21}^2 + 4\,G\,\Omega^2\right]^2} \stackrel{!}{=} 0. \tag{S13}$$

Solving for the frequency, we find the corresponding position of the peak maximum ω_{max}. The quadratic equation implies two solutions, one of which going to be non-physical, implying a negative resonance frequency (but mathematically necessary due to antiresonant contributions to the response function).

$$\omega_{max} = \sqrt{\omega_{21}^2 + \gamma_{21}^2 + 4G\Omega^2}. \tag{S14}$$

Two things are striking: (i) the position of the maximum is growing upon higher field strength (*via* Ω). (ii) Even in the linear regime ($\Omega = 0$), the resonance maximum of extended Kubo-Greenwood formula is depending on the dephasing rate coefficient γ_{21} itself. This is an artifact of the equilibration current[12], leading to vanishing DC mobility. Only, when the natural dephasing is small vs. the intrinsic resonance (i.e. $\omega_{21} > \gamma_{21}$) the position of the resonance maximum coincides with the eigenfrequency of the two-level system

$$\lim_{\substack{\Omega\to 0 \\ \omega_{21}\gg\gamma_{21}}} \omega_{max} = \omega_{21}. \tag{S15}$$

Now, reinserting Equation S14 back into S12, we are capable of describing the resonance maximum as a function of the system properties as well as experimental input as given by Equation (22) from the main text.

Likewise, we determine the full width at half maximum (FWHM) by solving for the frequency positions fulfilling the condition

$$\mathrm{Re}\left\{\mu_{2LS}\right\} \stackrel{!}{=} \frac{1}{2}\mathrm{Re}\left\{\mu_{2LS}(\omega_{max})\right\}. \tag{S16}$$

We

S3. NONLINEAR CONTRIBUTION TO THE DENSITY MATRIX

From evaluation of the frequency-dependent mobility in Eq. (16), we realize that only off-diagonal elements off the density matrix contribute to the expectation value. For that reason our main concern when calculating third order mobility, is tied to third order polarization as well. Reducing our discussion, as indicated in the main text, to a two level system, we start by setting $q = 3$ in Eq. (17) and write for the time-dependent third order polarization

$$\dot{\rho}_{21}^{(3)} = -(\mathrm{i}\omega_{21} + \gamma_{21})\rho_{21}^{(3)} + \frac{\mathrm{i}}{\hbar}\left(\rho_{11}^{(2)} - \rho_{22}^{(2)}\right) M_{21}E(t) + \frac{\mathrm{i}}{\hbar}\left[\sum_{n\neq 1}^{2} M_{2n}\rho_{n1}^{(2)} - \sum_{n\neq 2}^{2}\rho_{2n}^{(2)}M_{n1}\right] E(t) \tag{S17}$$

This Equation can be severely reduced by evaluating the actual sum, as we immediately recognize the entire bracket term to vanish due to the purely off-diagonal nature of the transition dipole matrix M. We write:

$$\dot{\rho}_{21}^{(3)} = -(\mathrm{i}\omega_{21} + \gamma_{21})\rho_{21}^{(3)} + \frac{\mathrm{i}}{\hbar}\left(\rho_{11}^{(2)} - \rho_{22}^{(2)}\right) M_{21}E(t). \tag{S18}$$

While the difference in population terms is usually tackled by invoking the closure relation $\rho_{11} + \rho_{22} = 1$, we need to reexamine this assumption in light of perturbation expansion.

As before, we write $\rho_{ij} = \rho_{ij}^{(0)} + \lambda\rho_{ij}^{(1)} + \lambda^2\rho_{ij}^{(2)} + \lambda^3\rho_{ij}^{(3)}$, which is supposed to hold for each and every element of ρ likewise. After insertion and rearranging, we find for the closure relation in perturbation theory

$$\rho_{11}^{(0)} + \rho_{22}^{(0)} = 1 \tag{S19}$$

$$\rho_{11}^{(1)} + \rho_{22}^{(1)} = 0 \tag{S20}$$

$$\rho_{11}^{(2)} + \rho_{22}^{(2)} = 0 \tag{S21}$$

$$\rho_{11}^{(3)} + \rho_{22}^{(3)} = 0. \tag{S22}$$

This does in no way mean that the perturbation elements themselves are vanishing, instead, they simply evolve pairwise, so that the second order population elements (as demanded in Equation S18 above) relate *via* $\rho_{11}^{(2)} = -\rho_{22}^{(2)}$. Ergo, Equation S18 simplifies as:

$$\dot{\rho}_{21}^{(3)} = -(\mathbb{i}\omega_{21} + \gamma_{21})\rho_{21}^{(3)} - 2\frac{\dot{\mathbb{i}}}{\hbar}\rho_{22}^{(2)}M_{21}E(t). \tag{S23}$$

At this point we introduce the population expansion equation according to our relaxation model - again in two-level approximation, we write

$$\dot{\rho}_{22}^{(2)} = \frac{\dot{\mathbb{i}}}{\hbar}\left(\rho_{21}^{*(1)} - \rho_{21}^{(1)}\right)M_{21}E(t) + \Gamma_{21}\rho_{11}^{(2)} - \rho_{22}^{(2)}\Gamma_{12}. \tag{S24}$$

Applying the perturbation closure relation reduces the Equation to

$$\dot{\rho}_{22}^{(2)} = \frac{\dot{\mathbb{i}}}{\hbar}\left(\rho_{21}^{*(1)} - \rho_{21}^{(1)}\right)M_{21}E(t) - (\Gamma_{21} + \Gamma_{12})\rho_{22}^{(2)}. \tag{S25}$$

From there, we are left with the first order perturbation expansion of the polarization element ρ_{21}. This is a crucial step, as it traces the expansion series down to an exactly solvable equation - either in the time or frequency domain. Again, we revisit Equation (17) from the main text and formulate the 1^{st} order polarization evolution equation.

$$\dot{\rho}_{21}^{(1)} = -(\mathbb{i}\omega_{21} + \gamma_{21})\rho_{21}^{(1)} + \frac{\dot{\mathbb{i}}}{\hbar}\left(\rho_{11}^{(0)} - \rho_{22}^{(0)}\right)M_{21}E(t). \tag{S26}$$

Identifying the 0^{th} order perturbation element as the corresponding thermal equilibrium density matrix element, i.e. $\rho_{ij}^{(0)} = \rho_{ij}^{eq}$, we can define the mutually affecting polarization-population series: Although we could easily solve this series in the time domain, we step into to the frequency domain, as this already favors the later description of frequency-dependent mobility. Starting off with the 1^{st} order term, we write by Fourier transforming using $FT\left\{\dot{\rho}_{21}(t)\right\} = -\mathbb{i}\omega\tilde{\rho}_{21}(\omega)$:

$$-\mathbb{i}\omega\tilde{\rho}_{21}^{(1)} = -(\mathbb{i}\omega_{21} + \gamma_{21})\tilde{\rho}_{21}^{(1)} + \frac{\dot{\mathbb{i}}}{\hbar}\left(\rho_{11}^{eq} - \rho_{22}^{eq}\right)M_{21}\tilde{E}(\omega). \tag{S27}$$

Solving the equation, we arrive at

$$\tilde{\rho}_{21}^{(1)}(\omega) = \frac{\dot{\mathbb{i}}}{\hbar}\frac{\left(\rho_{11}^{eq} - \rho_{22}^{eq}\right)M_{21}}{\mathbb{i}(\omega_{21} - \omega) + \gamma_{21}}\tilde{E}(\omega). \tag{S28}$$

$$\dot{\rho}_{21}^{(1)} = -(\mathbb{i}\omega_{21} + \gamma_{21})\rho_{21}^{(1)} + \frac{\mathbb{i}}{\hbar}\left(\rho_{11}^{eq} - \rho_{22}^{eq}\right) M_{21}E(t)$$
$$\Downarrow$$
$$\dot{\rho}_{22}^{(2)} = \frac{\mathbb{i}}{\hbar}\left(\rho_{21}^{*(1)} - \rho_{21}^{(1)}\right) M_{21}E(t) - (\Gamma_{21} + \Gamma_{12})\rho_{22}^{(2)}$$
$$\Downarrow$$
$$\dot{\rho}_{21}^{(3)} = -(\mathbb{i}\omega_{21} + \gamma_{21})\rho_{21}^{(3)} - 2\frac{\mathbb{i}}{\hbar}\rho_{22}^{(2)} M_{21}E(t)$$

In order to use this equation in the higher order population, we need to use the FT again. However, Equation S25 contains the time domain products $\rho_{21}^{*(1)}E(t)$ and $\rho_{21}^{(1)}E(t)$, so that the Fourier transform implies a convolution integral in the frequency domain. We start with

$$\tilde{\rho}_{22}^{(2)}(\omega) = \frac{\mathbb{i}}{\hbar}\frac{M_{21}\int\left(\tilde{\rho}_{21}^{*(1)}(-\omega') - \tilde{\rho}_{21}^{(1)}(\omega')\right)\tilde{E}(\omega-\omega')\mathrm{d}\omega'}{(\Gamma_{21}+\Gamma_{12}) - \mathbb{i}\omega}. \tag{S29}$$

where we made use of the FT property saying $\mathrm{FT}\left\{\rho_{21}^{*}(t)\right\} = \tilde{\rho}_{21}^{*}(-\omega)$ (since $\rho_{21}(t)$ itself is a complex quantity). Comparing Equation S28 and S29, we need to evaluate the term $\left(\tilde{\rho}_{21}^{*(1)}(-\omega') - \tilde{\rho}_{21}^{(1)}(\omega')\right)$:

$$\begin{aligned}
\tilde{\rho}_{21}^{*(1)}(-\omega') - \tilde{\rho}_{21}^{(1)}(\omega') &= -\frac{\mathbb{i}}{\hbar}\frac{\left(\rho_{11}^{eq} - \rho_{22}^{eq}\right)M_{21}}{-\mathbb{i}(\omega_{21}+\omega') + \gamma_{21}}\tilde{E}^{*}(-\omega') - \frac{\mathbb{i}}{\hbar}\frac{\left(\rho_{11}^{eq} - \rho_{22}^{eq}\right)M_{21}}{\mathbb{i}(\omega_{21}-\omega') + \gamma_{21}}\tilde{E}(\omega') \\
&= -\frac{\mathbb{i}}{\hbar}M_{21}\left(\rho_{11}^{eq} - \rho_{22}^{eq}\right)\left[\frac{1}{-\mathbb{i}(\omega_{21}+\omega') + \gamma_{21}} + \frac{1}{\mathbb{i}(\omega_{21}-\omega') + \gamma_{21}}\right]\tilde{E}(\omega') \\
&= -2\frac{\mathbb{i}}{\hbar}M_{21}\left(\rho_{11}^{eq} - \rho_{22}^{eq}\right)\frac{\gamma_{21} - \mathbb{i}\omega'}{\omega_{21}^{2} + (\gamma_{21} - \mathbb{i}\omega')^{2}}\tilde{E}(\omega'),
\end{aligned} \tag{S30}$$

Here, the same FT rule as above led to $\mathrm{FT}\left\{E(t)\right\} = \tilde{E}^{*}(-\omega) = \tilde{E}(\omega)$, since the electric field is a real-valued quantity. Given the elaboration above, we can plug the term into Equation S29 and conclude

$$\begin{aligned}
\tilde{\rho}_{22}^{(2)}(\omega) = &-2\left(\frac{\mathbb{i}}{\hbar}\right)^{2}M_{21}^{2}\left(\rho_{11}^{eq} - \rho_{22}^{eq}\right)\times \\
&\int\left(\frac{1}{2(\Gamma_{21}+\Gamma_{12}) - \mathbb{i}\omega}\right)\left(\frac{\gamma_{21} - \mathbb{i}\omega'}{\omega_{21}^{2} + (\gamma_{21} - \mathbb{i}\omega')^{2}}\right)\tilde{E}(\omega')\tilde{E}(\omega-\omega')\mathrm{d}\omega'.
\end{aligned} \tag{S31}$$

Lastly, we need to express the third order polarization element in the frequency domain starting from Equation S23

$$\tilde{\rho}_{21}^{(3)}(\omega) = -2\frac{\mathbb{i}}{\hbar}M_{21}\frac{1}{\mathbb{i}(\omega_{21}-\omega) + \gamma_{21}}\int\tilde{\rho}_{22}^{(2)}(\omega')\tilde{E}(\omega-\omega')\mathrm{d}\omega', \tag{S32}$$

so that we arrive - after inserting Equation S31 above - at Equation (24) given in the main text. We have to keep in mind that the mutual insertion of different expressions containing convolution integrals requires to rename the integration variable in order not

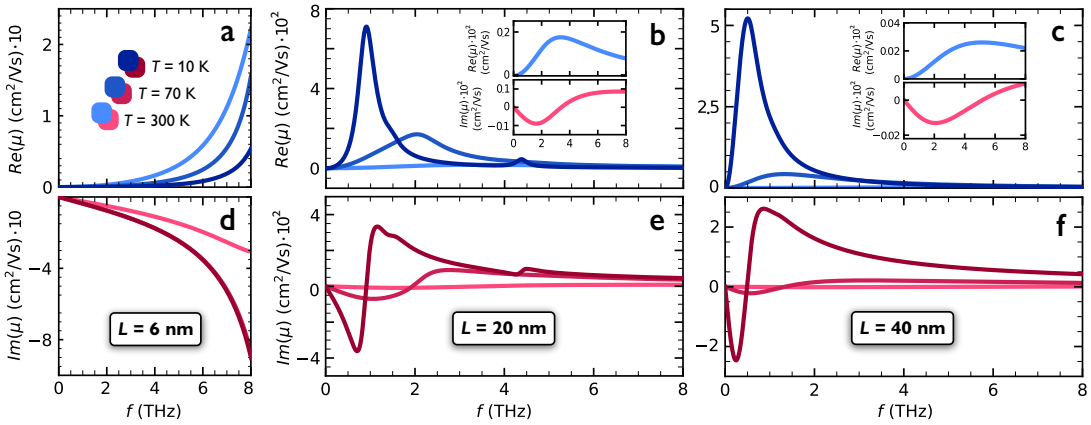

FIG. S1. Size dependence of real (a,b,c) and imaginary (d,e,f) hole mobility for $6 \times 6 \times 6\,\mathrm{nm}^3$, $20 \times 6 \times 6\,\mathrm{nm}^3$ and $40 \times 6 \times 6\,\mathrm{nm}^3$ CdSe quantum dots and wires at 10 K, 70 K and 300 K and a weak THz field with $E_0 = 0.1$ kV/cm, $\omega_0 = 2\pi{\times}1$ THz, a = -3, $\phi = 0$ and $\tau_{fwhm} = 0.5$ ps.

to lose the actual mathematical meaning. We write:

$$\tilde{\rho}_{21}^{(3)}(\omega) = 4\left(\frac{\mathbb{i}}{\hbar}\right)^3 M_{21}^3(\rho_{11}^{eq} - \rho_{22}^{eq})\,\frac{1}{\mathbb{i}(\omega_{21}-\omega)+\gamma_{21}}\times \tag{S33}$$
$$\iint\left(\frac{1}{(\Gamma_{21}+\Gamma_{12})-\mathbb{i}\omega'}\right)\left(\frac{\gamma_{21}-\mathbb{i}\omega''}{\omega_{21}^2+(\gamma_{21}-\mathbb{i}\omega'')^2}\right)\tilde{E}(\omega'')\tilde{E}(\omega'-\omega'')\tilde{E}(\omega-\omega')\mathrm{d}\omega''\mathrm{d}\omega',$$

which is equivalent to

$$\tilde{\rho}_{21}^{(3)}(\omega) = 4\left(\frac{\mathbb{i}}{\hbar}\right)^3 M_{21}^3(\rho_{11}^{eq} - \rho_{22}^{eq})\,\frac{\tilde{R}(\omega)}{\mathbb{i}(\omega_{21}-\omega)+\gamma_{21}} \tag{S34}$$

after introducing the lineshape distortion function $\tilde{R}(\omega)$ as done in the main text.

S4. CONTRIBUTION OF HOLE

Similar to the corresponding section from the main text, we want to shed some light on the transport of photogenerated holes in the nanostructures discussed. Given the different effective mass and deformation potential, this results in changed energy levels of the states as well as a differing initial population distribution from the Fermi-Dirac statistic and different up- and down-scattering rates. The frequency dependent mobility spectra for a hole in nanorods of different lengths and temperatures are shown in FIG. S1 analogously to the main text. A more complete picture is shown in FIG. S2 taking the sum of the electron contributions as presented in the main text and the hole contributions as seen in FIG. S1. Since the electron resonances are at a higher frequencies than those of the hole, FIG. S2 (a) and (d) for $L = 6$ nm remain almost unchanged compared to FIG. 1 (a) and (d). Similarly, FIG. S2 (c) and (f) for $L = 40$ nm only add a minor change to

the electron mobility while the hole contribution stands out for FIG. S2 (b) and (e), as there is less overlap between the peaks.

Because the hole mobility contributions are typically found at lower frequencies, their impact on the total absolute mobility is more prone to being reduced due to the quantum mechanical equilibration current which suppresses the mobility at low frequencies [13]. Since only four states have been considered in this numerical model also for holes, meant to focus on the field-dependence of the THz mobility, the results presented here have to be considered approximations in the case of holes. Alternative models using Kubo-Greenwood based approaches partially address this problem are [14] and [12], however to the detriment of being limited to the linear transport regime. The consideration of holes becomes increasingly relevant for small nanostructures, especially at lower temperatures, as electron transition energies move outside the typically investigated low (0-3) THz range in experiments. However, we would like to point out that the intention of our paper is to introduce the methodology of nonlinear charge transport simulation on a quantum mechanical basis with a focus on electron charge carriers.

---

[1] M.-Z. Huang and W. Ching, Journal of Physics and Chemistry of Solids **46**, 977 (1985).

[2] D. Langer, R. Euwema, K. Era, and T. Koda, Physical Review B **2**, 4005 (1970).

[3] J. Planelles, F. Rajadell, and J. I. Climente, The Journal of Physical Chemistry C **120**, 27724 (2016).

[4] Y. M. Sirenko, J.-B. Jeon, K. Kim, M. Littlejohn, and M. Stroscio, Physical Review B **53**, 1997 (1996).

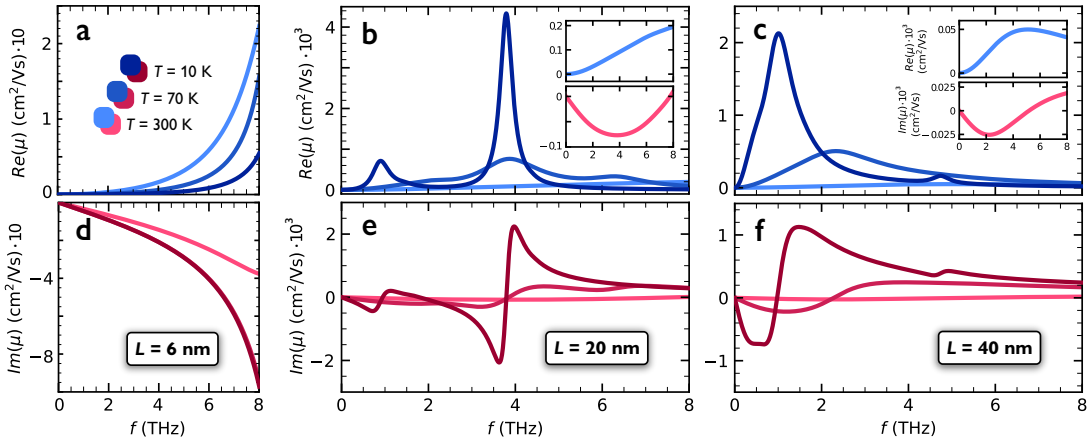

FIG. S2. Size dependence of the combined real (a,b,c) and imaginary (d,e,f) mobility of the electron and hole for $6 \times 6 \times 6\,\mathrm{nm}^3$, $20 \times 6 \times 6\,\mathrm{nm}^3$ and $40 \times 6 \times 6\,\mathrm{nm}^3$ CdSe quantum dots and wires at 10 K, 70 K and 300 K and a weak THz field with $E_0 = 0.1$ kV/cm, $\omega_0 = 2\pi \times 1$ THz, a = -3, $\phi = 0$ and $\tau_{fwhm} = 0.5$ ps.

[5] C. F. Cline, H. L. Dunegan, and G. W. Henderson, Journal of Applied Physics **38**, 1944 (1967).

[6] J. F. Specht, R. Scott, M. C. Castro, S. Christodoulou, G. H. Bertrand, A. V. Prudnikau, A. Antanovich, L. D. Siebbeles, N. Owschimikow, I. Moreels, *et al.*, Nanoscale **11**, 12230 (2019).

[7] M. C. Beard, G. M. Turner, and C. A. Schmuttenmaer, Nano Letters **2**, 983 (2002), https://doi.org/10.1021/nl0256210.

[8] P. Guyot-Sionnest, B. Wehrenberg, and D. Yu, The Journal of Chemical Physics **123**, 074709 (2005), https://pubs.aip.org/aip/jcp/article-pdf/doi/10.1063/1.2004818/15372154/074709_1_online.pdf.

[9] M. Makkar, L. Moretti, M. Maiuri, G. Cerullo, and R. Viswanatha, Journal of Physics: Materials **4**, 034005 (2021).

[10] T. Takagahara, Phys. Rev. Lett. **71**, 3577 (1993).

[11] A. W. Achtstein, S. Ayari, S. Helmrich, M. T. Quick, N. Owschimikow, S. Jaziri, and U. Woggon, Nanoscale **12**, 23521 (2020).

[12] M. T. Quick and A. W. Achtstein, The Journal of Physical Chemistry C **127**, 24591 (2023).

[13] M. T. Quick, Q. Wach, N. Owschimikow, and A. W. Achtstein, Advanced Photonics Research **4**, 2200243 (2023).

[14] A. W. Achtstein, N. Owschimikow, and M. T. Quick, Nanoscale **14**, 19 (2022).